

Inverse modeling of HEM data using a new inversion algorithm

A.R. Arab-Amiri^{1*}, A. Moradzadeh¹, N. Fathianpour², B. Siemon³

1. Faculty of Mining, Petroleum and Geophysics, Shahrood University of Technology, Shahrood, Iran.

2. Faculty of Mining Engineering, Isfahan University of Technology (IUT), Isfahan, Iran.

3. Federal Institute for Geosciences and Natural Resources (BGR), Hannover, Germany

Received 23 January 2010; received in revised form 26 November 2010; accepted 26 May 2011

*Corresponding author: aamiri@gsi.ir (A.R. Arab-Amiri).

Abstract

Helicopter-borne frequency-domain electromagnetic (HEM) surveys are used extensively for mineral and groundwater exploration and a number of environmental investigations. To have a meaningful interpretation of the measured multi-frequency HEM data, in addition to the resistivity maps which are provided for each frequency or for some particular depth levels, it is a necessity to have a suitable modeling technique to produce resistivity cross-sections along some specific profiles. This paper aims to: (1) develop a new inversion method to handle HEM data; (2) compare its results with the well known Amplitude, Niblett-Bostick (NB), and Siemon inversion methods. The basic formulation of this new inversion routine was provided based on the Zonge spatial filtering procedure to cure static shift effect on the magnetotelluric (MT) apparent resistivity curves. When the relevant formulas and the required algorithm for the inverse modeling of HEM data were provided, they were then coded in Matlab software environment. This new inversion program, named as SUTHEM, was used to invert some sets of one and two dimensional (1D and 2D) model synthetic data which were contaminated by random noise. It was also applied to invert one set of real field data acquired in the NW part of Iran by the DIGHEM system. The obtained results of this method and their comparison with those of the aforementioned methods indicate that SUTHEM is able to produce the results like those produced by established Siemon routines. In addition, the new inversion method is superior to the Amplitude and the NB methods particularly in inversion of the noisy data.

Keywords: HEM data inversion, MT, DIGHEM, resistivity model, SUTHEM.

1. Introduction

Today geophysical surveys play important roles in mineral, water and hydrocarbons exploration. They are also used in engineering sites investigation and lately in environmental studies. Geophysical exploration is being done by various methods in which electromagnetic (EM) is one of these methods that have high performance and capability. Considering the physical induction law, various EM methods have been introduced to implement exploration in both time and frequency domains for ground and airborne surveys [1]. Modern frequency domain airborne electromagnetic (AEM) systems utilize small transmitter and receiver coils. A sinusoidal current flow through the transmitter coil generates a primary magnetic field at each frequency that is very close

to a dipole field at some distance from the transmitter coil. The oscillating primary magnetic field induces eddy currents in the subsurface of the earth. These currents, in turn, generate the secondary magnetic field, which is related to the earth resistivity distribution. The induced secondary magnetic field is measured by the receiver coil and related to the primary magnetic field expected at the centre of the receiver coil. As the secondary field is very small with respect to the primary field, the primary field is generally bucked out and the relative secondary field is measured in parts per million (ppm) [2]. Due to the induction process within the earth, there is a small phase shift between the primary and secondary field, i.e., the relative secondary magnetic field is a complex quantity [3]. In practice, the transmitter coil is horizontal (VMD:

vertical magnetic dipole) or vertical (HMD: receiver coil is oriented in a maximally coupled position, resulting in horizontal coplanar, vertical coplanar, or vertical coaxial coil systems. Among various types of AEM methods, helicopter-borne electromagnetic (HEM) is the method where the transmitting and measuring system (bird) is towed at a sufficiently large distance below the helicopter and is kept at about 30–40 m above ground level (Figure 1).

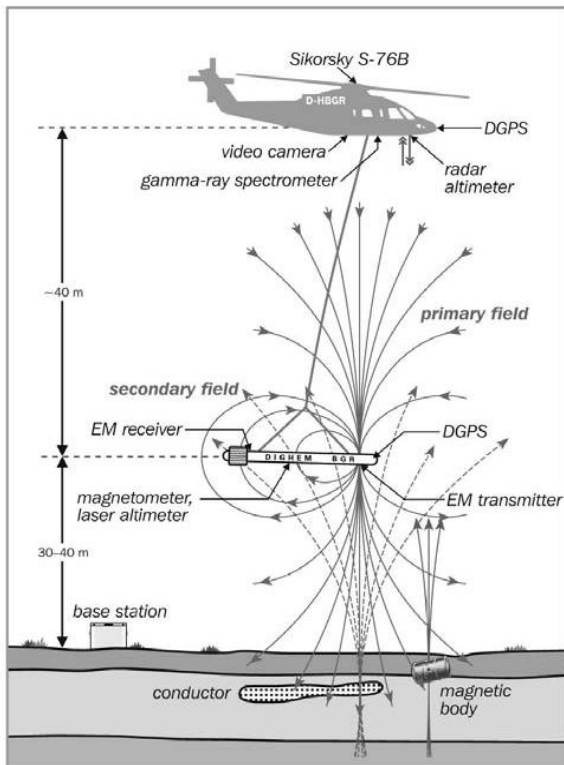


Figure 1. A helicopter-borne geophysical system: Electromagnetic, magnetic, GPS and laser altimeter sensors are housed in a “bird”, a cigar-shaped 9 m long tube, which is kept at about 30–40 m above ground level. The gamma-ray spectrometer, additional altimeters and the navigation system are installed into the helicopter.

In this configuration this method is capable enough to survey and acquire high quality data within a few days in remote, rough, and vast regions.

Several research groups in the world try to receive new modeling methods and new survey tools [4]. In frequency domain HEM method, the final results are shown as resistivity maps or resistivity depth sections of the subsurface along the survey lines [5]. The vertical sections are constructed by concatenating the resistivity models for every measuring point along a survey line using the topographic relief as base line in meter above

horizontal magnetic dipole) and the mean sea level. Several methods exist for getting these results.

Inverse modeling was started with Fraser’s algorithm in 1978 [6]; then Mundry [7] invented an algorithm for the improved numerical calculation in 1984; and a short time later, Sengpiel presented an algorithm for depth calculation so-called “centroid depth” in 1988 [8]. In addition to its high speed of calculation, it does not require an initial guess of resistivity variation for inversion. The main drawback of this method is the inaccurate estimation of the true depth of subsurface structures. This method was improved using a new, effective depth, parameter [9]. It seems that the precision of this method is more than that of the Sengpiel’s method in the detection of deep conductors. In 1997 Siemon introduced an improvement on Sengpiel’s centroid depth and also introduced a new method to get the resistivity and depth of subsurface structures using differentiating of HEM resistivity data with respect to the measuring frequencies [5,10]. As the Niblett-Bostick (NB) transformation was used to achieve the goal, it is also called NB inversion method [5]. This approach is more sensitive to the conductor depth relative to the previously developed methods and also does not require bird altitude which is often inaccurate, but it requires an initial model. After using the aforementioned methods in the inversion of HEM data and specifying their advantages and disadvantages in different practical cases, several other inversion algorithms were introduced by Siemon in 1997. These are called Amplitude, Epsilon and Combined methods. Despite these improvements there are still some limitations to acquire precise depth and resistivity of the subsurface structures along the survey lines. In this paper, the researchers aim to develop a new and improved approach to model the HEM data so that it could partially compensate some limitations of the previously developed methods.

2. Basic formulas

2.1. Secondary magnetic field calculation

The secondary magnetic field over a stratified subsurface, caused by an oscillating magnetic dipole source in the air, is calculated using well-known formulae [11, 12]. They are based on Maxwell’s equations and solve the homogeneous induction equation in the earth for the electromagnetic field vector F .

$$\frac{d^2 F}{dz^2} = v^2 F \quad (1)$$

$$v^2 = \lambda^2 + i\omega\mu\sigma - \omega^2\mu\varepsilon$$

where σ , is the conductivity of a homogeneous and isotropic earth, $\omega=2\pi f$ is the angular frequency, λ is the wave number, and $i = \sqrt{-1}$ is the imaginary unit. Magnetic effects and displacement currents are normally neglected.

For a horizontal-coplanar (HCP) coil pair with a coil separation r and at an altitude h above the surface, the relative (normalized) secondary magnetic field Z ($\frac{Z_s}{Z_p} = (R + iQ)$) is given as follows [7, 11]:

$$Z = r^3 \int_0^\infty R_0(f, \lambda, \rho(z)) \lambda^2 e^{-2\lambda h} J_0(\lambda r) d\lambda \quad (2)$$

in which Z is complex and normalized secondary magnetic field, Z_s and Z_p are complex secondary and primary field, R and Q are respectively real (in phase) and quadrature (out of phase) components of Z , r is the horizontal distance between transmitter and receiver coils, R_0 is reflection factor containing the underground vertical resistivity distribution $\rho(z)$ with z pointing downwards, h is sensor height above ground and J_0 and J_1 are Bessel functions of first kind and zero or first order, respectively and can be approximated as follows:

$$J_0(x) \cong 1 - \frac{x^2}{4} + \frac{x^4}{64} - \dots \quad (3)$$

$$J_1(x) \cong \frac{x}{2} - \frac{x^3}{16} + \frac{x^5}{384} - \dots \quad (4)$$

$$J_0(x) \cong 1 - \frac{x^2}{4} + \frac{x^4}{64} - \dots$$

Similar relations are given as equation (5) for vertical-coplanar (VCP) and equation (6) for vertical-coaxial (VCA) coil array.

$$Y = r^2 \int_0^\infty R_0(f, \lambda, \rho(z)) \lambda e^{-2\lambda h} J_1(\lambda r) d\lambda \quad (5)$$

$$X = r^2 \int_0^\infty R_0(f, \lambda, \rho(z)) \lambda e^{-2\lambda h} \frac{J_1(\lambda r) - \lambda J_0(\lambda r)}{2} d\lambda \quad (6)$$

while $r < 0.3h$, the horizontal secondary field values perpendicular (Eq. 5) and along (Eq. 6) the transmitter-receiver direction can be approximated by $Y \approx Z/2$ and $X \approx -Z/4$, respectively [6]. Thus, only Z is regarded in the following.

The reflection factor of homogeneous half space with resistivity ρ below an air layer is given as follow:

$$R_0 = \frac{\lambda - v}{\lambda + v}, \quad v = \sqrt{\lambda^2 + \frac{2i}{p^2}}, \quad p = \sqrt{\frac{2\rho}{\omega\mu_0}} \quad (7)$$

where $\omega=2\pi f$ is the angular frequency, $\mu_0 = 4\pi \times 10^{-7}$ (Vs/Am) is the magnetic permeability of free space and P is the skin depth. Several methods exist for solving the complex integrals in Eqs. 2, 5, and 6 [5]. The fast Hankel transform [13, 14] and the very fast Laplace transform [15] are two popular methods which are being used routinely to solve the integrals numerically.

3. Inverse modeling of HEM data with transformation to the homogeneous half space parameters

One important stage of the HEM data interpretation is the calculation of the resistivity and its corresponding depth. As the dependency of secondary field to the half space resistivity is highly non-linear (Eq. 2), the resistivity calculation is possible by using iterative inverse modeling, curve fitting and look up table. In the case of a layered half-space, the true resistivity distribution can be approximated by a resistivity-depth, $\rho_a(z)$, sounding curve which is derived by presenting the apparent resistivity ρ_a for each frequency at the corresponding depth values [5]. In multi-frequency HEM surveys the sensor height h and the two components of the secondary magnetic field (i.e. R and Q) are measured at each frequency. Therefore, the corresponding apparent resistivity, ρ_a , can be obtained by using two of these three measured parameters [6]. As the real, R , response is very small for great penetration depths and that the quadrature response, Q , peaks at an intermediate depth, thus it is not recommended to use the real or quadrature response alone for obtaining the apparent resistivity together with the available sensor height. Furthermore, the sensor height maybe affected by trees or buildings, hence both real and quadrature components of the normalized secondary magnetic field are normally required to calculate the apparent resistivity at each frequency precisely. In the latter routine the apparent resistivity, ρ_a , and the calculated sensor height or apparent distance, D_a , will be the results of modeling. The apparent distance is the distance between sensor and the top of the conducting half space.

Over a homogeneous half-space ground, the calculated sensor height equals the measured sensor height h . For an inhomogeneous layered half-space, however, the apparent resistivity is an approximation to the true resistivity of the ground.

In this case, the measured sensor height h is not necessarily equal to the calculated sensor height D_a . The difference between the calculated and the measured sensor height is called the apparent depth and defined as [6]:

$$d_a = D_a - h \quad (8)$$

Considering the real and quadrature components, amplitude ($A = |Z| = \sqrt{R^2 + Q^2}$), and phase ratio $\varepsilon = Q/R$ of the measured data, the apparent resistivity and its corresponding depth are calculated by using some graphs [5] that illustrate logarithmic variation of transformed amplitude, $A'^{1/3} = A^{1/3}/\gamma$ (where $\gamma = r/h$) or $\log \varepsilon$ versus $\log \delta$ ($\delta = h/p$). The apparent resistivity is obtained from the definition of skin depth (Eq. 7) using the following relations:

$$\delta = \frac{h}{p} \Rightarrow p = \frac{h}{\delta} = \sqrt{\frac{2\rho}{\omega\mu_0}} \Rightarrow \rho_a = (h/\delta)^2 \left(\frac{\omega\mu_0}{2}\right) \quad (9)$$

Therefore, if the amplitude or the phase ratio or both of them are used for obtaining the apparent resistivity at each frequency, their corresponding resistivity is depicted as $\rho_a^A, \rho_a^\varepsilon, \rho_a^C$, respectively. In the latter combined approach (combining R and Q data), besides calculating the apparent resistivity, the apparent EM sensor height, h_a , which is equivalent of the apparent distance, D_a , is also calculated from the ratio of transformed A' and the measured amplitude A:

$$h_a = r \left(\frac{A'}{A}\right)^{1/3} \equiv D_a \quad (10)$$

A resistivity-depth profile, can be obtained if the apparent resistivity is displayed for each measured frequency versus a specific depth, the centroid depth $z^*(f)$. The centroid depth was introduced by Schmucker [16, 17] for the interpretation of MT data. It is interpreted as the centre of depth of the in-phase current system [18]. Similarly, concept of centroid depth was firstly applied in the HEM data interpretation by Sengpiel in 1988 [8]. After this, an improved centroid depth based on the apparent skin depth was introduced to precisely locate the buried conductivity structures. It was defined as $Z^* = d_a + \frac{p_a}{2}$ [5]. Once the resistivity

and its relevant depth have been calculated at all frequencies and measuring points, the resistivity–depth profiles or their resistivity cross sections could be constructed for each survey profile.

It has been shown that differentiation of the apparent resistivity with respect to the depth or

frequency is more effective than the previously explained methods [5, 9]. In this paper, however, the differentiation of the apparent resistivity with respect to frequency is explained and coded to apply on HEM data. This method was firstly introduced to enhance 1D inversion of magnetotelluric data by incorporating MT phase data [18]. The measured HEM phase $\varphi_\varepsilon = \tan^{-1}(Q/R)$, is not, however, comparable with the MT phase. In a homogeneous half-space model, for example, it varies from $0-\pi/2$ for HEM survey, while it has a constant value of $\pi/4$ in MT measurement. Hence, a new parameter corresponding to the MT phase is being sought to apply known MT methods to HEM data. Weidelt [18] approximated the phase of MT data by differentiating the apparent resistivity with respect to frequency:

$$\varphi_a(f) \approx \frac{\pi}{4} \left(1 + \frac{f}{\rho_a(f)} \frac{d\rho_a(f)}{df}\right) \quad (11)$$

It is called apparent phase in HEM data analysis against the measured phase, φ_ε , data. Now considering Eq. (11), a new apparent resistivity formula is defined using the NB transformation [19, 20]:

$$\rho_{NB} = \rho_a \frac{1+m(f)}{1-m(f)}, \quad m(f) = \frac{d \log(\rho_a)}{d \log(f)} = \frac{f}{\rho_a} \frac{d\rho_a}{df} = m' \left(\frac{m'+c}{1+c}\right) \quad \text{and} \quad m' = 1 - \frac{4}{\pi} \varphi_a \quad (12)$$

The derivative $d\rho_a/df$ is numerically determined by differentiating a spline interpolation curve through the $\rho_a(f)$ values. It has been found that Eq. (12) with $c=3\log(5)$ ensures that $|m| < 1$ for realistic resistivity distributions [5, 21].

The $\rho_{NB}(f)$ resistivity sounding curve is more sensitive to greater depth compared with the $\rho_a(f)$ sounding curve, thus, a new depth parameter is required to display the ρ_{NB} values at a proper depth [5]:

$$Z_S^* = d_a + \frac{p_a}{\sqrt{2}} \quad (13)$$

This method hereafter is referred to as the NB inversion in HEM data interpretation. The algorithm of this method, together with the amplitude, epsilon and combined (R and Q) methods have been developed and coded in Matlab software to invert the component of secondary magnetic field in each frequency. The obtained results are then compared with those taken by a newly developed inversion method called SUTHEM. This method is explained bellow.

4. Introducing an improved method of inversion for HEM data

As this method was developed at Shahrood University of Technology (SUT) for inversion of HEM data, it has been abbreviated as SUTHEM modeling algorithm. The foundation of this routine relates to the spatial filtering technique that was introduced by Zonge [22] for static shift correction of MT apparent resistivity sounding curve. In this method, a static-corrected resistivity data, ρ_c , is derived by integrating of the static-free phase data for each sounding station as bellow:

$$\rho_c = \rho_N \exp \left[-\frac{4}{\pi} \int_{f_H}^{f_L} \left(\varphi - \frac{\pi}{4} \right) d \ln f \right] \quad (14)$$

where ρ_N is the constant of integration (the static offset or normalizing value), f_H and f_L are the highest and lowest survey frequency respectively, and φ is the E/H phase difference [22]. This study attempts to modify Eq.14 for the first time so that it could be used to obtain resistivity data from the measured HEM data using a reference or initial resistivity model. The required initial resistivity model, ρ_N , of each station could be obtained by any of the aforementioned HEM inversion schemes, such as the combined (R and Q) method as described by Siemon [5]. Thus we have $\rho_N = \rho_S$. Now Eq. 14 reduced to:

$$\rho_z = \rho_s \exp \left[-\frac{4}{\pi} \int_{f_H}^{f_L} \left(\varphi - \frac{\pi}{4} \right) d \ln f \right] \quad (15)$$

where ρ_z is Zonge apparent resistivity, and ρ_s is Siemon apparent resistivity. As phase, φ , of each station varies with varying survey frequency, we have $\tan \varphi = Q/R$ and the value of phase for each specific point and frequency, for example at the first point and the first frequency, is given as: $\varphi = \tan^{-1}(Q_1/R_1)$. Therefore Eq. 15 changes to Eq. 16:

$$\rho_z = \rho_s \exp \left[-\frac{4}{\pi} \left(\tan^{-1} \left(\frac{Q}{R} \right) - \frac{\pi}{4} \right) \int_{f_H}^{f_L} d \ln f \right] \quad (16)$$

We can write:

$$\int_{f_H}^{f_L} d \ln f \approx \ln f \quad (17)$$

As the range of HEM frequency is very large, for each survey frequency, f , the lower, f_1 , and the upper, f_2 , limits of the above integral is described as the upper and lower neighboring values of measuring frequency. Now in such limiting conditions by substituting the value of $(\int_{f_H}^{f_L} d \ln f)$ from Eq. 17 in Eq. 16, the following formula is defined to produce a new apparent resistivity, ρ_{SUT} , at each frequency:

$$\rho_{SUT} = \rho_s \exp \left[-\frac{4}{\pi} \left(\tan^{-1} \left(\frac{Q}{R} \right) - \frac{\pi}{4} \right) (\ln f_1 - \ln f_2) \right] \quad (18)$$

For the modeling of HEM data, however, two parameters of apparent resistivity and their corresponding depth value are required at each frequency to contribute to a resistivity-depth curve. To determine the apparent depth related to the measured resistivity, the response of variety of different synthetic layered models were inverted by several depth relations such as;

$$Z_{SUT}^* = d_a + \frac{P_a}{2} \quad [5], \quad Z_{SUT}^* = d_a + \frac{P_a}{\sqrt{3}} \quad [23], \quad \text{and}$$

$$Z_{SUT}^* = d_a + \frac{P_a}{\sqrt{2}} \quad [21] \quad \text{as illustrated in Figure 2. It}$$

has been found that the following formula is the best for depth calculation:

$$Z_{SUT}^* = d_a + \frac{P_a}{\sqrt{2}} \quad (19)$$

This proposed inversion method incorporates the improved Guptasarma-Singh forward core developed by authors in another research work [24, 25]. Its corresponding complete inversion computer codes were prepared in Matlab software and were used to invert both synthetic and real HEM data.

5. Results and discussion

In the following sections the performance of the proposed inversion method is evaluated with a series of 1D and 2D artificial models with and without the noise and finally the obtained results are compared with those acquired by the others inversion methods. This method is also used to invert the real DIGHEM HEM data acquired in the Kurdistan province, NW Iran.

5.1. Inverse modeling of synthetic HEM data

The synthetic HEM data of a three and a four-layer model were provided by our developed forward computer program. The model response was calculated in 15 frequencies within the range of 200 Hz to 200 kHz for a HEM system including HCP coils with separation of 8 meters and sensor height of 30 meters above the ground surface. The results of data inversion using SUTHEM and combined Siemon method are shown in Figure 3.

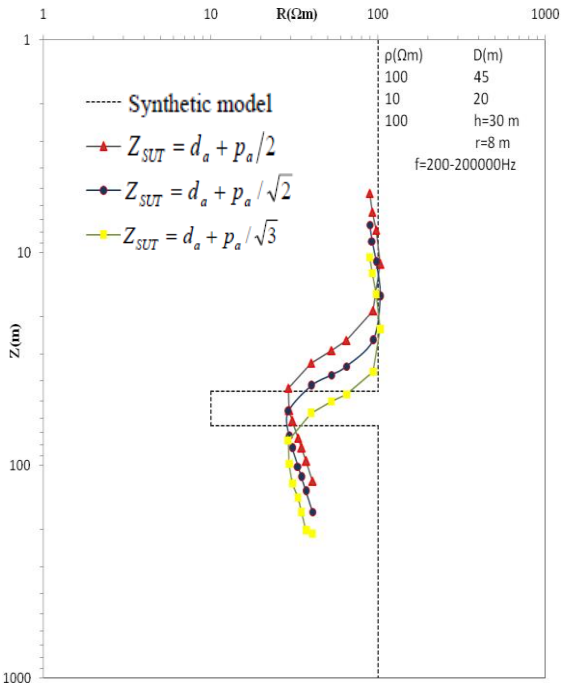


Figure 2. The results of synthetic HEM data inversion using SUTHEM method with different depth relations. It is seen that the new inversion method with depth relation given by Eq. 19 is able to recover the model.

As it can be seen, the results are in good agreement and both methods are able to detect the model parameters smoothly but the depth of SUTHEM method is greater in both smooth models.

In addition a 2D synthetic model (Figure 4.b) consisting of a four-layer model in which its upper layer contains a 2D conductive body of 50 Ωm with section of 100m×20m is considered for further comparison of the ability of SUTHEM and other inversion methods. Such a 2D model was also used in the many research work related to HEM data inversion [26, 27]. The third layer and the upper 2D body within the model are represented as a deep and shallow conductor, respectively. The synthetic HEM data sets (response of 2D model) were calculated with a step size of 5 m using the improved Guptasarma-Singh forward code (Figure 4.a). The computed anomalous secondary field values (R and Q components) are for a five-frequency ($f_5=387$, $f_4=1820$, $f_3=8225$, $f_2=41550$, and $f_1=133200$ Hz) horizontal-coplanar HEM system at a sensor altitude of $h = 30\text{m}$ and a coil separation of $r= 8\text{m}$. The computed response values are also given as the real and quadrature components of anomalous secondary field for each 10 m distance interval in each measuring frequencies (Table 1). The obtained results of SUTHEM inversion (Figure 4.f) are compared with the results of the amplitude

(Figure 4.c), combined Siemon (Figure 4.d), and NB (Figure 4.e) inversion methods.

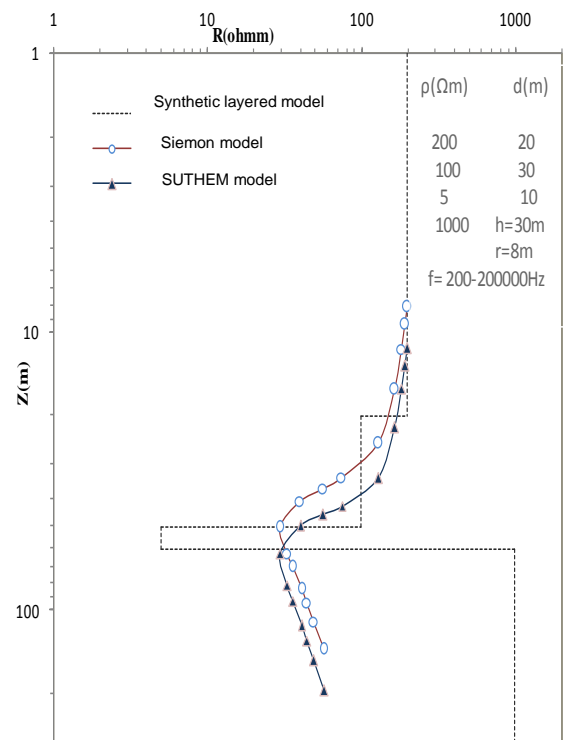
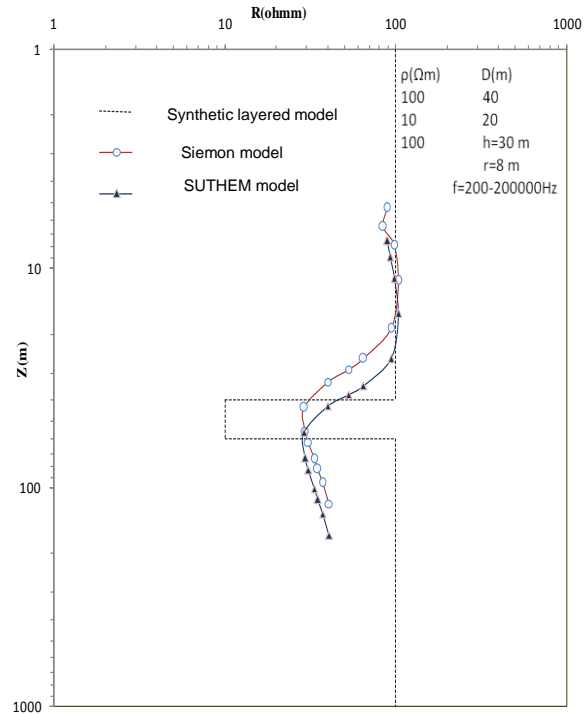


Figure 3. The results of inversion of SUTHEM and Siemon methods for three (above) and four layered (below) earth models.

As Figure 4 indicates, all four inversion methods are able to detect the depth and resistivity of the top layer (with resistivity of 200 Ωm) and also to locate the embedded 2D conductive body correctly. The lower boundaries of the upper and

its underneath layer are however recognized more precisely by the NB (Figure 4.e) and the SUTHEM (Figure 4.f) inversion procedures. It can also be seen that none of these inversion schemes is able to recognize precisely the resistivity of the thin conductive layer (5Ωm) situated at depth of 50 to 60m, except its effects is

slightly visible in resistivity section yielded by the NB (Figure 4.e) and the SUTHEM (Figure 4.f) inversion. The precise location and the resistivity of the deepest layer of the model could not be distinguished in none of the obtained resistivity models and this is possibly due to the very smooth nature of the inversion routines.

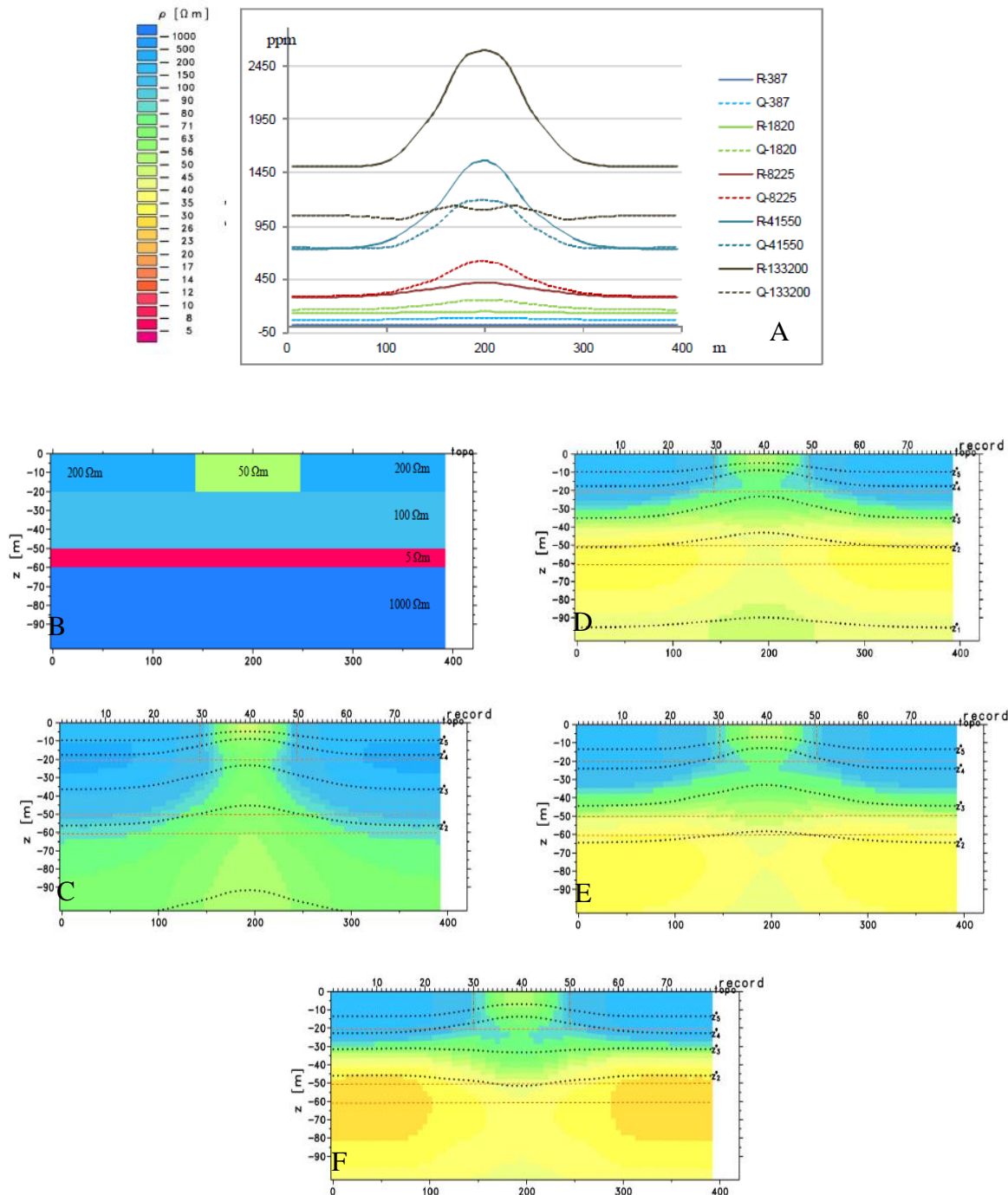


Figure 4. Inversion of synthetic HEM data: a) Anomalous HEM data (R and Q) for five frequencies, b) Four-layer resistivity model containing a 2 D conductive body of 50 Ωm in the top layer and a very conductive layer at the depth of 50-60 m., c) The results of amplitude inversion as a resistivity versus centroid depth cross-section, d) The results of combined Siemon inversion, e) The results of Niblett-Bostick inversion, f) The resistivity model created using the SUTHEM inversion. In all resistivity models black dots stand for centroid depth values and the boundaries of the original 2D model (orange dashed lines) are also overlain on all resistivity models.

Table 1. The computed HEM data (as real and quadrature components of the anomalous secondary magnetic field) of the 2D resistivity model shown in Figure 4a. The computed responses were provided by improved Guptasarma-Singh forward program for a five-frequency (387, 1820, 8225, 41550, and 133200 Hz) horizontal-coplanar HEM system at a sensor altitude of $h = 30\text{m}$ and a coil separation of $r = 8\text{ m}$.

X	R-387	Q-387	R-1820	Q-1820	R-8225	Q-8225	R-41550	Q-41550	R-133200	Q-133200
5	21.8	68.36	129.11	164.36	280.43	291.46	734.67	747.39	1505.9	1046.78
15	21.84	68.46	129.31	164.56	280.83	291.66	734.97	746.99	1505.9	1046.78
25	21.88	68.59	129.61	164.76	281.53	291.96	735.47	746.49	1505.9	1046.78
35	21.94	68.76	129.91	165.16	282.43	292.46	736.37	745.79	1506.9	1045.78
45	21.99	68.98	130.41	165.66	283.73	293.36	737.87	744.89	1506.9	1044.78
55	22.06	69.26	130.91	166.36	285.53	294.76	740.67	743.59	1507.9	1043.78
65	22.13	69.63	131.51	167.56	288.13	297.06	745.37	741.99	1509.9	1041.78
75	22.21	70.13	132.31	169.16	291.73	300.66	753.67	740.59	1512.9	1038.78
85	22.3	70.79	133.31	171.46	296.63	306.56	767.57	740.39	1521.9	1032.78
95	22.39	71.67	134.41	174.76	303.23	315.66	790.17	743.79	1538.9	1023.78
105	22.5	72.83	135.61	179.46	311.73	329.56	824.87	754.79	1574.9	1014.78
115	22.6	74.32	137.01	185.66	322.33	349.36	873.87	779.29	1638.9	1012.78
125	22.7	76.09	138.51	193.26	334.33	375.06	935.07	819.99	1736.9	1027.78
135	22.78	77.95	139.81	201.36	346.43	403.46	1001.37	870.09	1849.9	1060.78
145	22.85	79.74	141.01	209.26	357.83	432.26	1070.37	919.79	1960.9	1086.78
155	22.91	81.8	142.11	218.46	369.73	467.96	1160.37	985.59	2106.9	1109.78
165	22.98	84.44	143.31	230.56	384.13	516.06	1286.37	1074.69	2300.9	1133.78
175	23.05	87.12	144.61	242.76	399.93	564.86	1417.37	1146.69	2467.9	1131.78
185	23.11	89.13	145.61	251.86	413.13	600.46	1512.37	1181.69	2559.9	1112.78
195	23.14	90.1	146.21	256.26	420.03	617.36	1557.37	1191.69	2592.9	1100.78
205	23.14	89.95	146.11	255.56	418.93	614.76	1550.37	1189.69	2588.9	1102.78
215	23.1	88.68	145.41	249.76	410.03	592.66	1491.37	1175.69	2541.9	1117.78
225	23.03	86.43	144.21	239.56	395.63	552.36	1383.37	1130.69	2428.9	1134.78
235	22.96	83.65	143.01	226.96	379.83	501.66	1248.37	1048.69	2243.9	1127.78
245	22.9	81.15	141.81	215.56	366.23	456.36	1131.37	962.69	2056.9	1100.78
255	22.83	79.23	140.71	206.96	354.73	423.76	1049.37	904.39	1926.9	1079.78
265	22.76	77.44	139.51	199.06	343.13	395.46	982.57	855.29	1816.9	1049.78
275	22.67	75.59	138.11	191.06	330.93	367.56	917.47	807.19	1706.9	1020.78
285	22.57	73.89	136.71	183.86	319.33	343.46	859.37	771.09	1618.9	1011.78
295	22.47	72.49	135.31	178.06	309.33	325.36	814.27	750.79	1562.9	1016.78
305	22.37	71.41	134.11	173.86	301.33	312.86	783.17	742.29	1532.9	1026.78
315	22.27	70.59	133.01	170.76	295.13	304.76	763.17	740.19	1518.9	1033.78
325	22.19	69.98	132.11	168.66	290.63	299.56	751.07	740.89	1511.9	1039.78
335	22.11	69.52	131.31	167.16	287.33	296.36	743.87	742.39	1508.9	1042.78
345	22.04	69.18	130.71	166.16	285.03	294.36	739.77	743.89	1507.9	1044.78
355	21.98	68.91	130.21	165.46	283.33	293.06	737.47	745.19	1506.9	1045.78
365	21.92	68.71	129.81	164.96	282.13	292.36	736.07	746.09	1506.9	1045.78
375	21.87	68.55	129.51	164.66	281.33	291.86	735.27	746.69	1505.9	1046.78
385	21.83	68.43	129.31	164.46	280.73	291.56	734.87	747.09	1505.9	1046.78
395	21.79	68.34	129.11	164.36	280.33	291.36	734.57	747.39	1505.9	1046.78

The obtained results indicate that the depth of investigation for the SUTHEM inversion is the same as the NB method and it is deeper than the depth of the other inversion procedure considered in this study.

In practice, noise is part of the measured data and its nature and value depend on to the geological and survey conditions. Therefore, it is necessary to verify the stability and robustness of each HEM inversion scheme. To achieve this goal, a homogeneous half space synthetic resistivity model with $10\ \Omega\text{m}$ resistivity (Figure 5.b) is considered and its HEM responses (R and Q components) are calculated with an interval

spacing of 1 m (Figure 5.a) for the same HCP five-frequency bird system. To realize noisy data, a set of 1–5% random noise was added to the calculated HEM data of the lowest to highest frequency, and the contaminated data were then inverted using different methods. The random noise was added to the synthetic data so that the first measuring point above the homogenous half- space ground, zero position on the top of the model (Figure 5.b), is noise free, the next ten points contain 1% noise, the second ten points include 2% noise, the third ten points have 3% noise, the fourth ten points consist of 4% noise and finally the last ten points have 5% noise. The results of each individual 1D

inversion of the contaminated HEM data along the 5 profiles with 51 data sets have been assembled and then demonstrated for the amplitude

(Figure 5.c), Siemon (Figure 5.d), NB (Figure 5.e) and SUTHEM (Figure 5.f) techniques.

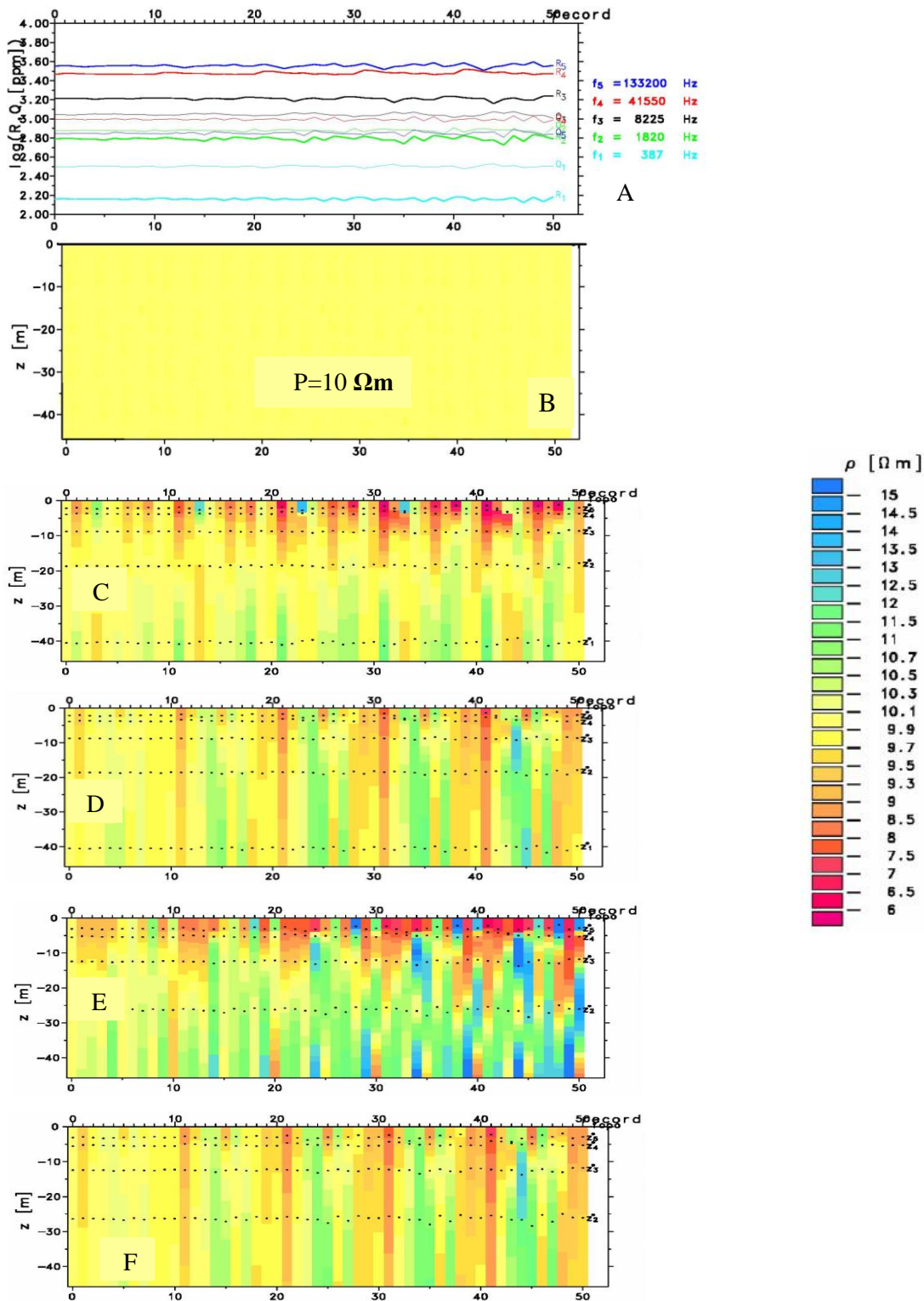


Figure 5. Inversion of synthetic HEM (1-5%) randomly added noisy data: a) The calculated HEM data (R and Q) for a HCP five frequency system, b) A half-space 10 Ωm resistivity model, c) The results of amplitude inversion as a resistivity-depth section, d) The results of combined Siemon inversion, e) The results of Niblett-Bostick inversion, f) The resistivity model created using the SUTHEM inversion. In all resistivity models black dots stand for centroid depth values.

In all 2D resistivity sections (Figure 5), the value of 10 Ω m resistivity was shown as yellow color, thus the stability of different inversion methods is recognized in the presence of noise with a glance to see how the colored bars are changing in 2D resistivity sections. Once color varies from yellow to blue or pink (considering colored resistivity legend of Figure 5), the stability of modeling with respect to noise is reduced. Thus in this set-up, a multicolored resistivity section indicates an unstable inversion of HEM data. Consequently, the modeling of noisy HEM data (Figure 5.c-f) shows that the NB modeling provides a model with least stability whereas the SUTHEM method yields the most stable resistivity model.

5.2. Inversion of real field data

Finally this method was used to invert a set of real DIGHEM field data related to the Barika area, in the Kurdistan province, NW Iran (Figure 6). The obtained results (Figure 7.c) were then compared with those attained by the Siemon (Figure 7.a) and Niblett-Bostick (Figure 7.b) methods. The geological map (Figure 6) of the study area indicates a set of faulted, sheared and argillitic altered zones which contain trace of gold, copper and zinc mineralization. A careful attention to the resistivity model obtained by the SUTHEM method (Figure 7.c) and its comparison with those yielded by the other inversion schemes and also to the geological section (Figure 7.d) show that these low resistivity zones coincide to the Barika and Shamula sheared and mineralized zones in the left section of the model. In addition, in the right part of the SUTHEM model another set of low resistivity zones are revealed that are possibly related to the faulted areas shown in the geological map, whereas these conductive zones are not detected in the results of Siemon model (Figure 7.a) and they are illustrated weakly with noisy pattern in the NB resistivity section (Figure 7.b).

6. Conclusions

In the present study a new inversion method has been developed to interpret HEM data. This technique is called SUTHEM. The basic formulation of this technique relates to the Zonge spatial filtering approach for MT static shift correction, of course with some modifications. Once its complete formulation and inversion algorithm has been provided, the necessary

inversion codes were written in the Matlab software by incorporating of an improved Guptasarma-Singh forward core. This method has then been applied on a variety of 1D and 2D synthetic model data containing up to 5% random noise and also one set of real HEM data. The results of inversion in all cases have been compared with those produced by the well known Siemon, Amplitude, and Niblett-Bostick inversion algorithms. The results of inversion for the noisy synthetic and field data indicate that the SUTHEM method is superior to the other used inversion methods. Furthermore, it was found that the obtained model of real field data is capable enough to identify the conductive zones related to the possible sheared mineralization zones.

Acknowledgment

We would like to thank Dr. U. Meyer (Federal Institute for Geosciences and Natural Resources (BGR)) for the numerous fruitful helps and J. Pielawa (BGR) for preparing a few figures.

References

- [1]. Telford, W.M., Geldart, L.P., and Sheriff, R.E., (1990). Applied Geophysics, second edition, Cambridge university press, 770 pp.
- [2]. Siemon, B. (2006). Electromagnetic methods – frequency domain: Airborne techniques. In: Kirsch, R. (ed.), Groundwater Geophysics – A Tool for Hydrogeology, Springer-Verlag, Berlin, Heidelberg, 155-170.
- [3]. Siemon, B. (2009). Levelling of helicopter-borne frequency-domain electromagnetic data. J Appl. Geophys, 67: 209-221.
- [4]. Fugro Airborne Surveys Inc. (2003). Airborne electromagnetic surveys short course. <http://www.fugroairborne.com>,
- [5]. Siemon, B. (2001). Improved and new resistivity depth profiles for helicopter electromagnetic data. J Appl. Geophys, 46: 65–76.
- [6]. Fraser, D.C. (1978). Resistivity mapping with an airborne multi-coil electromagnetic system. Geophys, 43: 144–172.
- [7]. Mundry, E. (1984). On the interpretation of airborne electromagnetic data for the two-layer case. Geophys. Prospect., 32: 336–346.

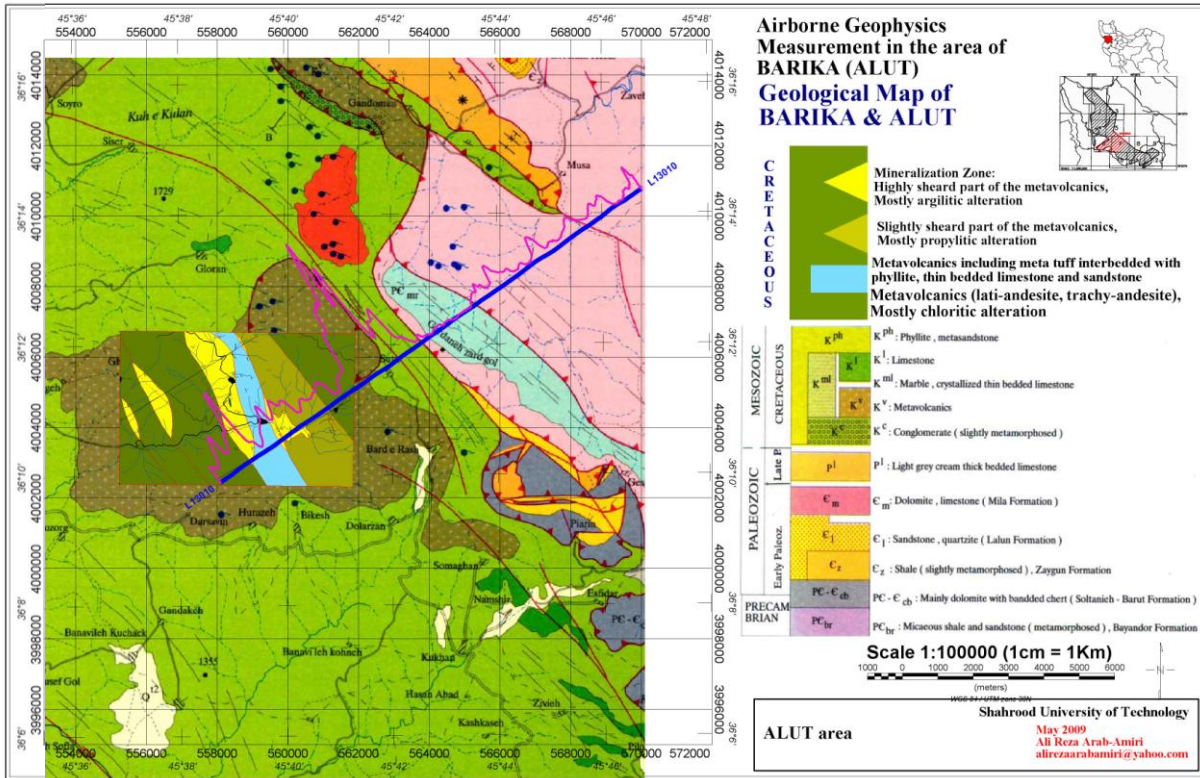


Figure 6. Part of 1:100000 geological map of Alut area in Kurdistan province, NW Iran on which a 1:10000 geological map of around Barika area and a path of HEM survey line with real component of anomalous secondary magnetic field variation for frequency 7210 Hz have been overlaid.

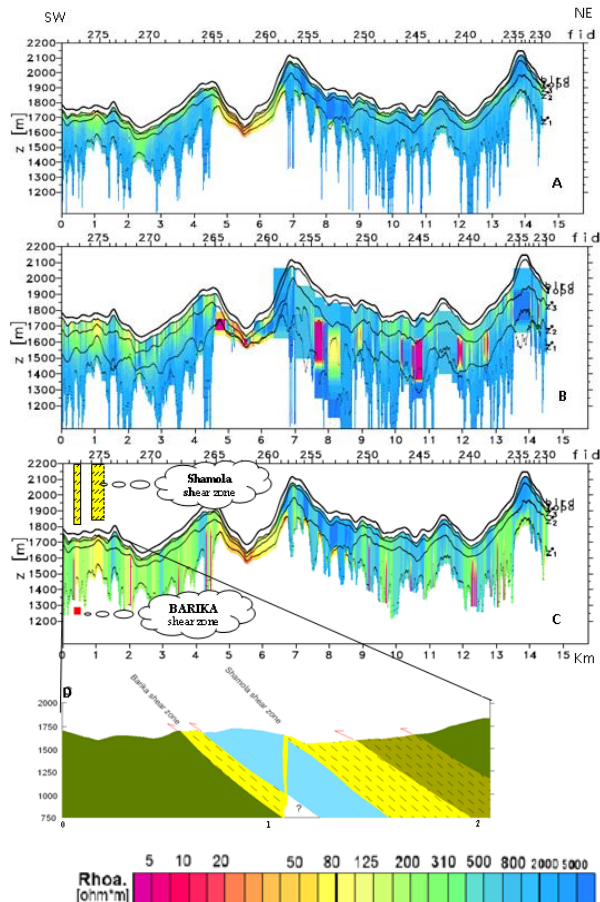


Figure 7. The resistivity models obtained by the inversion of HEM data acquired along a 15 Km profile around Barika mining districts and part of Alut area: a) The results of combined Siemon inversion, b) The results of Niblett-Bostick inversion, c) The resistivity model created using the SUTHEM inversion, d) The geological section along the first 2 Km part of HEM profile.

[8]. Sengpiel, K.P. (1988). Approximate inversion of airborne EM data from a multi-layered ground. *Geophys. Prospect.*, 36: 446-459.

[9]. Huang, H. and Fraser, D.C. (1996). The differential parameter method for multifrequency airborne resistivity mapping. *Geophys.*, 61:100-109.

[10]. Siemon, B. (1997). *Verbesserte Algorithmen zur Bestimmung von Sondierungskurven in der Hubschrauber elektromagnetik*. Bundesanstalt für Geowissenschaften und Rohstoffe, Report No. 115920, Hannover, unpublished., 81 pp.

[11]. Wait, J.R. (1982). *Geo-Electromagnetism*, Academic Press Inc., New York.

- [12]. Ward, S.H. and Hohmann, G.W. (1987). Electromagnetic theory for geophysical applications. In: Nabighian, M.N. (Ed.), *Electromagnetic Methods in Applied Geophysics, Theory*, Vol 1, Investigations in Geophysics No. 3. Society of Exploration Geophysicists (SEG), Tulsa, pp. 131–311.
- [13]. Anderson, W.L. (1982). Fast Hankel Transforms Using Related and Lagged Convolutions. *ACM T. Math. Software (TOMS)*, 8: 344-368.
- [14]. Johanson, H.K. and Sørensen, K. (1979). Fast Hankel transforms. *Geophys. Prospect.*, 27: 876–901.
- [15]. Fluche, B. and Sengpiel, K.-P. (1997). Grundlagen und Anwendungen der Hubschrauber-Geophysik. In: Beblo, M. (Ed.), *Umweltgeophysik*, Ernst und Sohn, Berlin, pp. 363–393.
- [16]. Schmucker, U. (1970). Anomalies of geomagnetic variations in the southwestern United States. *Bull. Scripps Inst. Oceanogr.* 13: 1–165, La Jolla, CA.
- [17]. Schmucker, U. (1971). Neue Rechenmethoden zur Tiefen-sondierung. In: Weidelt, P. _Ed., *Protokoll über das Kolloquium A Erdmagnetische Tiefen-sondierung B in Rothenberge*, University of Gottingen, pp. 1–39.
- [18]. Weidelt, P. (1972). The inverse problem of geomagnetic induction. *Z. f. Geophys.*, 38: 257-289
- [19]. Jones, A.G. (1983). On the equivalence of the Niblett and Bostick transformations in the magnetotelluric method. *Geophys.*, 38: 72-73.
- [20]. Schmucker, U. (1987). Substitute conductors for electromagnetic response estimates. *Pure Appl. Geophys (PAGEOPH)*, 125: 341–367.
- [21]. Sengpiel, K.-P. and Siemon, B. (2000). Advanced inversion methods for airborne electromagnetic exploration. *Geophys.*, 65: 1983–1992.
- [22]. Zonge, K.L. and Hughes, L. J. (1993). Controlled source audio-frequency magnetotellurics. In: Nabighian, M.N. (Ed.). *Electromagnetic Methods in Applied Geophysics- Vol 2, Applications, Part A and Part B*. Society of Exploration Geophysicists (SEG), 972 p.
- [23]. Meng, Q. and Hu, P. (2006). Frequency-domain airborne electromagnetic approximate inversion and application. *SEG Annual Meeting*, New Orleans, USA.
- [24]. Arabamiri, A.R., Moradzadeh, A., Rajabi, D., Fathianpour, N. and Siemon, B. (2010). Investigation of forward modeling accuracy in HEM data inverse modeling. *Scientific Q J Geosciences 20 (77)*: 137-140. (In Persian).
- [25]. Arabamiri, A.R., Moradzadeh, A., Rajabi, D., Siemon, B. and Fathianpour, N. (2010). Definition and comparison of improved Mundry's integral on HEM data inverse modeling. *Scientific Q J Geosciences*, 19 (75): 115-118. (In Persian).
- [26]. Siemon, B., Auken, E. and Christiansen, A.V. (2009). Laterally constrained inversion of helicopter-borne frequency-domain electromagnetic data. *J Appl. Geophys.*, 67: 259–268.
- [27]. Hodges, G., and Siemon, B. (2008). Comparative analysis of one-dimensional inversion of helicopter-borne frequency-domain electromagnetic data. *Proc, 5th Intl Conference on Airborne Electromagnetics, AEM2008*, Haikko Manor, Finland.